Rb₂ diffuse band emission excited by diode lasers

T. Ban[a], D. Aumiler, R. Beuc, and G. Pichler

Institute of Physics, Bijenička 46, P.O. Box 304, 10001 Zagreb, Croatia

Abstract. We investigated collisional processes involved in the population of the Rb₂ diffuse band through resonant excitation of Rb atoms. Near-infrared (780 nm) and violet (420 nm) diode lasers were used for the Rb first ($5\,^2S_{1/2} \rightarrow 5\,^2P_{3/2}$) and second ($5\,^2S_{1/2} \rightarrow 6\,^2P_{3/2}$) resonant doublet excitations. Laser induced fluorescence spectra were detected and investigated at different rubidium densities, buffer gas pressures and excitation wavelengths.

PACS. 33.80.Gj Diffuse spectra; predissociation, photodissociation – 33.50.Dq Fluorescence and phosphorescence spectra – 33.20.Kf Visible spectra

1 Introduction

Dense alkali metal vapors offer rich spectra and many interesting spectral phenomena. Among them, diffuse bands of the alkali dimers have been widely investigated in absorption [1,2] and emission [3–6] measurements. They are identified as $2\,^3\Pi_g \rightarrow 1(a)\,^3\Sigma_u^+$ free-free and bound-free triplet transitions [2,5–7]. On that account they were proposed for achieving laser action in alkali metals [8–11]. In the last five years alkali diffuse bands were used as a first step in REMPI detection of ultracold alkali molecules [12–15].

The emission spectra of alkali diffuse bands populated through direct laser excitation or different atom-molecule collisions were extensively investigated (see Ref. [3]). Na₂ and K₂ diffuse bands were observed by resonance line excitation of Na and K atoms in references [16–19]. The authors discussed several mechanisms, which could participate in the population of the $2\,^3\Pi_g$ state, but the dominant mechanism still remained unconfirmed. The diffuse band emission has also been observed in the spectra of glow and high pressure discharges [20,21], although the concentration of molecules in the vapor is much smaller compared to the concentrations of atoms and ions. The authors in references [10,22] proposed the Na₂ $2\,^3\Pi_g$ state population by dissociative recombination of Na₃⁺ ions. The production of Na₃⁺ ions as a result of associative ionization (AI) of Na($4d, 5s$) atoms and ground state Na₂ dimers was measured in reference [23]. The experiment was performed in a single effusive sodium atomic beam. Na₃⁺ dissociative recombination was followed by emission in the 425–460 nm wavelength range, which corresponds, to sodium violet diffuse band emission [24]. The production of Na₃⁺ ions in a single supersonic beam via AI molecule-atom collisions,

with the molecules and atoms in their first excited states was investigated in references [25,26]:

$$\mathrm{Na}(3p) + \mathrm{Na}_2(1(A)\,^1\Sigma_u^+) \rightarrow \mathrm{Na}_3^+ + e^-. \qquad (1)$$
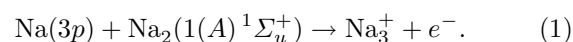
To our knowledge, semiconductor diode lasers until now have not been used in studies of laser induced fluorescence (LIF) of the dense alkali vapors. In particular, the Rb₂ diffuse band emission has been observed by direct laser excitation [7] and argon-ion laser excitation lines [5]. Huennekens et al. [27] reported observation of the Rb₂ and Cs₂ diffuse bands by dye laser resonant excitation. However, the authors were primarily interested in the ionization and population of high-lying cesium and rubidium atomic states, without any detailed investigation of the diffuse bands. Our initial motivation was to take advantage of the diode lasers, namely their narrow line width, and investigate the diffuse band emission spectra in a less complex excitation scheme.

In this paper we observed the orange Rb₂ diffuse band by red and violet laser excitation of the Rb first ($5\,^2S_{1/2} \rightarrow 5\,^2P_{3/2}$) and second ($5\,^2S_{1/2} \rightarrow 6\,^2P_{3/2}$) resonant doublet. We investigated the dependence of the Rb₂ LIF spectrum upon vapor density, pressure of argon buffer gas, excitation wavelength and laser intensity. In addition, we performed high resolution excitation spectroscopy by scanning the wavelength of the Rb second ($5\,^2S_{1/2} \rightarrow 6\,^2P_{3/2}$) doublet excitation laser around 420 nm.

In the next section we present the outline of our experiment. The results of the both types of excitations are presented in Section 3. The discussion of the results is presented in Section 4. Finally, in Section 5 we give conclusions and stress the need for further experiments.

[a] e-mail: `ticijana@ifs.hr`
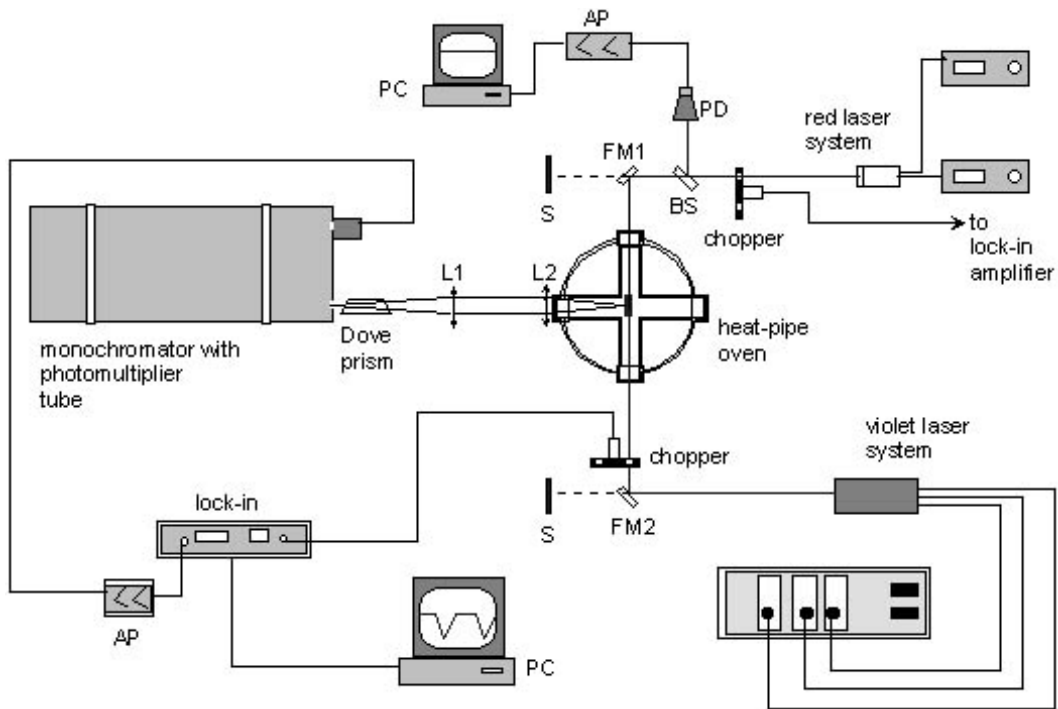
Fig. 1. Experimental set-up. AP – amplifier; L1, L2 – lenses, FM1, FM2 – folder mirrors, PD – photodiode, BS – beamspliter, S – beam stopper.

2 Experiment

The experimental arrangement used for Rb_2 diffuse band observation is shown in Figure 1. The rubidium vapor was generated in a crossed heat-pipe oven, made from two stainless steel pipes (140 mm and 170 mm long, with 16 mm inner diameter). The pipe ends were closed with quartz windows and connected to a vacuum system. The pressure of argon, used as a buffer gas, was controlled with an absolute pressure transducer (MKS Baratron 722A). A thermocoax heater wound around the center of the heat-pipe oven was connected to a stabilized power supply, providing stable temperature conditions of the system. The temperature was measured using a thermocoax thermocouple in contact with the mantle of the heat-pipe oven, as close to its center as possible. In the measurements, the pressure of argon buffer gas was varied from 10–100 Torr, which was much higher than the highest partial pressure of rubidium vapor, e.g. the measurements were not performed in the so-called heat-pipe mode of operation.

A free-running diode laser (HITACHI, HL7851G), with 40 mW of maximum output power was used for the excitation of the Rb D_2 line at 780 nm. The laser wavelength tuning was obtained by changing the current and temperature of the laser diode. The excitation of the second Rb D_2 line at 420 nm was performed by an external cavity diode laser system (ECDL, Toptica DL100 with NLHV3000E laser diode) [28,29]. Single mode operation was obtained in the 22 GHz tuning range with a maximum output power of 16 mW and a bandwidth of approximately 1 MHz.

LIF was observed perpendicularly to the laser beam and focused onto the entrance slit of the 1.5 m Jobin-Yvon THR scanning monochromator. The monochromator was equipped with a 1200 grooves/mm holographic grating. All LIF spectra were measured with 800 μm slit widths resulting in a resolution of 0.4 nm, which caused many molecular spectra to appear as continuum spectra. The holographic grating was rotated by means of a computer controlled stepper motor. The light at the exit slit of the monochromator was detected using a photomultiplier tube (Hamamatsu SR936). The signal was amplified by a lock-in amplifier (Stanford Research Systems SR510) connected to a mechanical light chopper and stored on a laboratory PC.

3 Results

Two different excitation schemes, presented in Figure 2, were employed for the diffuse band emission. Rb_2 potential curves calculated without the spin-orbit interaction were taken from reference [30]. In the first case, the excitation was performed with red diode laser tuned around the first resonant Rb D_2 line ($5\,^2S_{1/2} \rightarrow 5\,^2P_{3/2}$). In the second case, the violet diode laser was used to excite the second resonant D_2 line ($5\,^2S_{1/2} \rightarrow 6\,^2P_{3/2}$).

3.1 Red laser excitation

A LIF spectra of rubidium vapor at 547 K (rubidium pressure 0.54 Torr) excited by the laser light tuned to the near
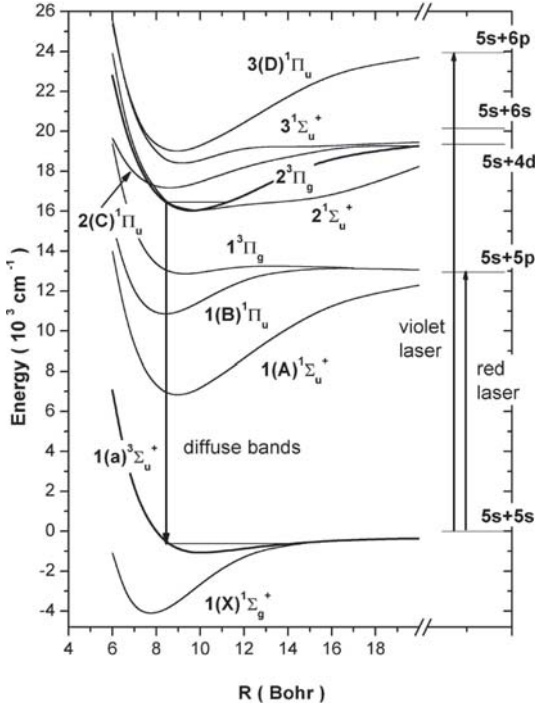
Fig. 2. Rb$_2$ potential curves and their molecular asymptotes relevant for the present experiment.
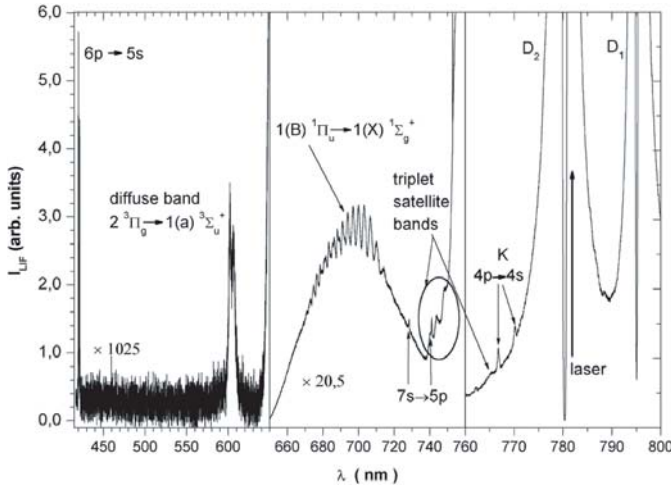
Fig. 3. The overall LIF spectra of rubidium vapor at 547 K ($N_{\mathrm{Rb}} = 9.5 \times 10^{15}$ cm^{-3}) excited by the laser located at 782 nm, $p(\mathrm{Ar}) = 52$ Torr.
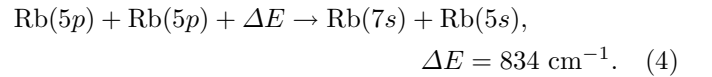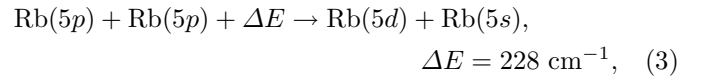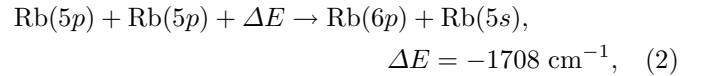
red wing of the first resonance D$_2$ line is shown in Figure 3. Vertical lines shown in the figure divide the spectra in three wavelength regions, regarding the intensity of the observed LIF signal. The argon gas pressure was 52 Torr, which was approximately the optimum for Rb$_2$ diffuse band observation. Different rubidium atomic and molecular features can be recognized in the spectra.

The atomic features consist of rubidium $6p \rightarrow 5s$ (420.2 nm, 421.6 nm), $7s \rightarrow 5p$ (728 nm, 740.8 nm), strong self-broadened first resonance D$_1$ and D$_2$, $5p \rightarrow 5s$, atomic emission lines and potassium $4p \rightarrow 4s$ reso-
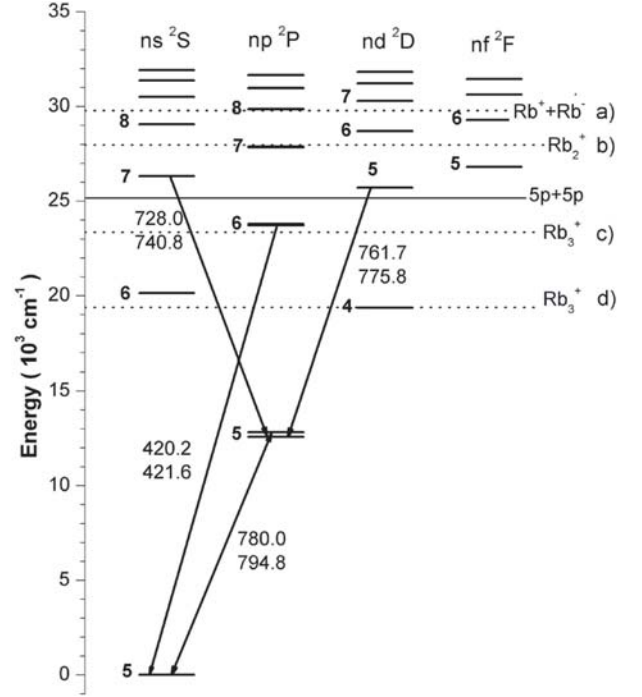

Fig. 4. Rubidium Grotrian energy level diagram. Dotted lines correspond to the threshold energies for: (a) ion-pair formation, (b) two-body associative ionization to dimer ion, (c) two-body associative ionization to trimer ion, (d) three-body associative ionization to trimer ion.

nance lines. The Rb($5\,^2$P$_{3/2}$) level is populated by absorption of a laser light located in the red wing of the D$_2$ line ($\lambda_{laser} = 782$ nm). The energy difference between the fine-structure levels of the $5p$ configuration is 237.6 cm^{-1}, so that the collisional energy transfer from $5\,^2$P$_{3/2}$ to $5\,^2$P$_{1/2}$ is a dominant mechanism for the Rb($5\,^2$P$_{1/2}$) level population. Rb($6p$), Rb($5d$) and Rb($7s$) levels are energetically close to the $5p + 5p$ molecular asymptotes, and therefore they are populated via energy pooling processes [31–33] described by the following relations:

$$\mathrm{Rb}(5p) + \mathrm{Rb}(5p) + \Delta E \rightarrow \mathrm{Rb}(6p) + \mathrm{Rb}(5s),$$
$$\Delta E = -1708 \text{ cm}^{-1}, \quad (2)$$

$$\mathrm{Rb}(5p) + \mathrm{Rb}(5p) + \Delta E \rightarrow \mathrm{Rb}(5d) + \mathrm{Rb}(5s),$$
$$\Delta E = 228 \text{ cm}^{-1}, \quad (3)$$

$$\mathrm{Rb}(5p) + \mathrm{Rb}(5p) + \Delta E \rightarrow \mathrm{Rb}(7s) + \mathrm{Rb}(5s),$$
$$\Delta E = 834 \text{ cm}^{-1}. \quad (4)$$

The energy defects ΔE are calculated from the energies of the corresponding atomic levels, omitting the fine-structure energies, taken from the Moore tables [34].
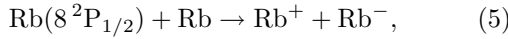
Along with the energy pooling, formation of atomic and molecular ions is also possible which can be visualized by inspecting the energy level diagram, Figure 4. The dotted lines correspond to the threshold energies with respect to the infinitely separated ground state atoms for the
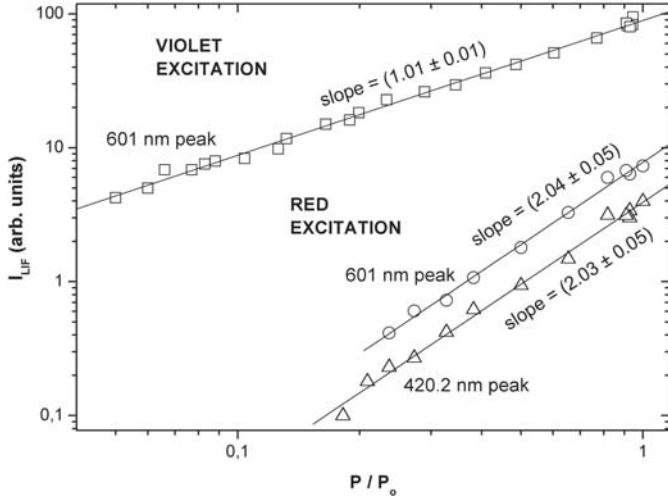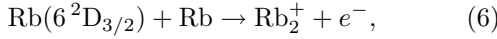
Fig. 5. Dependencies of the emission peaks intensities at 601 nm and 420.2 nm upon the power of the red and violet excitation lasers. 601 nm peak: squares – violet excitation, circles – red excitation. 420.2 nm peak – red excitation.
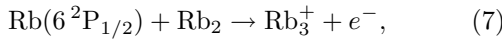
following processes (see Ref. [22]):
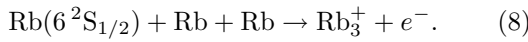
(a) ion-pair formation

$$\mathrm{Rb}(8\,^2\mathrm{P}_{1/2}) + \mathrm{Rb} \rightarrow \mathrm{Rb}^+ + \mathrm{Rb}^-, \qquad (5)$$

(b) two-body associative ionization to dimer ion

$$\mathrm{Rb}(6\,^2\mathrm{D}_{3/2}) + \mathrm{Rb} \rightarrow \mathrm{Rb}_2^+ + e^-, \qquad (6)$$

(c) two-body associative ionization to trimer ion

$$\mathrm{Rb}(6\,^2\mathrm{P}_{1/2}) + \mathrm{Rb}_2 \rightarrow \mathrm{Rb}_3^+ + e^-, \qquad (7)$$

(d) three-body associative ionization to trimer ion

$$\mathrm{Rb}(6\,^2\mathrm{S}_{1/2}) + \mathrm{Rb} + \mathrm{Rb} \rightarrow \mathrm{Rb}_3^+ + e^-. \qquad (8)$$

The dependence of the $6\,^2\mathrm{P}_{3/2} \rightarrow 5\,^2\mathrm{S}_{1/2}$ emission peak intensity at 420.2 nm upon the power of the excitation (red) laser shows quadratic behaviour, Figure 5, indicating that the energy pooling (2) is the dominant mechanism for populating $6p$ states of Rb atoms. This excludes three-photon ionization and subsequent recombination as the effective population mechanism of the $6\,^2\mathrm{P}_{3/2}$ level. The $7s \rightarrow 5p$ emission intensities were too small for such investigation. The processes described by relations (3) and (4) are endoergic. For the Rb vapor at 550 K ($kT \sim 382\,\mathrm{cm}^{-1}$) the faster atoms located in the tail of Maxwell velocity distribution contribute in the population of Rb($7s$) state via relation (4). The most resonant energy pooling reaction is one described by relation (3). However, in the LIF spectra shown in Figure 3, the $5d \rightarrow 5p$ emission intensities were heavily influenced by the optically thick vapor near the D_2 resonance.

The molecular features observed in the presented LIF spectrum are: $2\,^3\Pi_g \rightarrow 1(a)\,^3\Sigma_u^+$ (diffuse band), $1(B)\,^1\Pi_u \rightarrow 1(X)\,^1\Sigma_g^+$ band and triplet satellite bands.
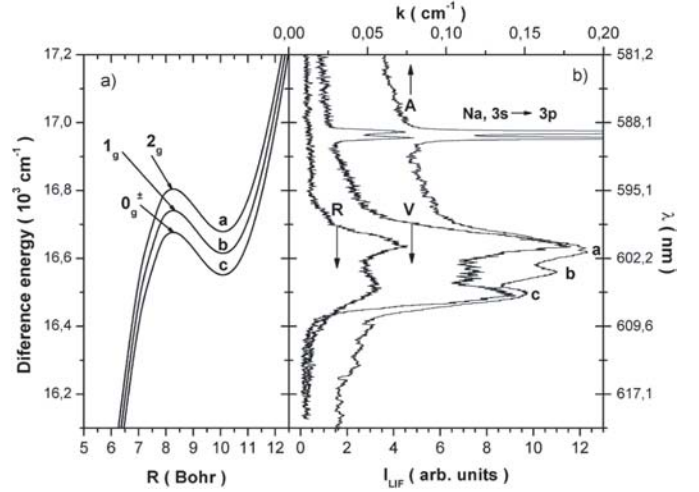
Fig. 6. (a) $\mathrm{Rb}_2\,2\,^3\Pi_g(2_g,1_g,0_g^\pm) - 1(a)\,^3\Sigma_u^+(1_u,0_u^-)$ difference potentials relevant for the explanation of diffuse band emission profiles. (b) Rb_2 diffuse band LIF spectra measured for the vapor at $T = 557$ K ($N_\mathrm{Rb} = 1.3 \times 10^{16}\,\mathrm{cm}^{-3}$) and $p(\mathrm{Ar}) = 22$ Torr excited by red (trace denoted with letter R) and violet (trace denoted with letter V) laser light positioned at the close wings of Rb first and second resonance D_2 line. Trace denoted with letter A is measured absorption coefficient for $T = 695$ K.

The Rb_2 long-range $1\,^3\Pi_g(2_g,1_g,0_g^\pm) \rightarrow 1(a)\,^3\Sigma_u^+(0_u^-,1_u)$ transitions known as triplet satellite bands are observed in the 735–781 nm wavelength range. For the full interpretation of absorption observations see reference [35]. $\mathrm{Rb}_2\,1(B)\,^1\Pi_u$ and $1\,^3\Pi_g$ molecular states are populated through energy transfer from excited atoms to molecules in the ground $(1(X)\,^1\Sigma_g^+)$ state [19] and in three-body recombination with noble gas atoms as third particles.

The Rb_2 diffuse band LIF spectrum in the 580–620 nm wavelength region, obtained after excitation by the red laser, at the temperature $T = 557$ K and with buffer gas pressure set at 22 Torr, is shown in more detail in Figure 6b (trace denoted by letter R). Diffuse band emission can be observed in the 519–615 K temperature range, corresponding to $4 \times 10^{15} - 5.4 \times 10^{16}\,\mathrm{cm}^{-3}$ rubidium atom concentration. The length of the vapor column was approximately 8 cm assessed by the length of the heated zone. The emission is characterized by two smooth peaks located approximately at 601 nm (higher intensity and narrower) and 605.5 nm (lower intensity and broader). The observed diffuse band emission profile is independent of the red laser excitation wavelength, the temperature of the vapor and the pressure of argon gas. The diffuse band emission maximum is obtained when the excitation laser wavelength is located conveniently either in the red or the blue wing of the D_2 resonance line. The dependence of the diffuse band maximum intensity (peak at 601 nm) on the power of the excitation laser exhibits quadratic behavior (circles in Fig. 5).
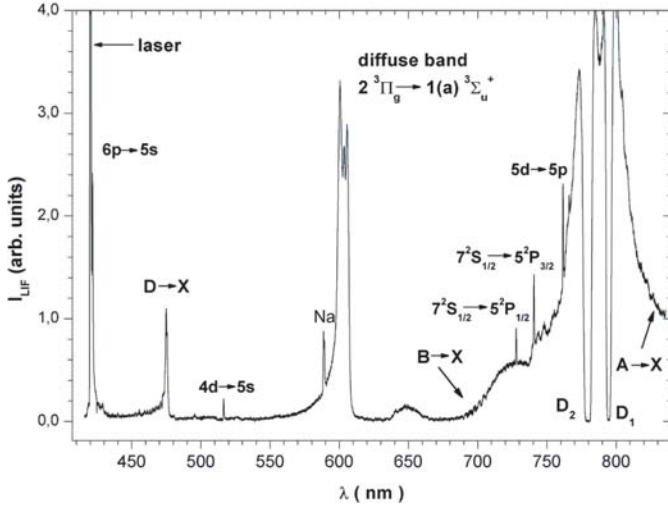
Fig. 7. The overall LIF spectra of rubidium vapor at 638 K ($N_{\mathrm{Rb}} = 8.9 \times 10^{16}$ cm^{-3}) excited by the violet laser light positioned at the center of the Rb D$_2$ second resonance doublet line.

3.2 Violet laser excitation

A LIF spectra of rubidium vapor at 638 K excited by violet laser light, whose wavelength is positioned in the center of Rb D$_2$ second resonance line is shown in Figure 7. The Rb D$_2$ second resonance line has a smaller transition probability then first resonance line, so the spectrum shown in Figure 7 is taken at much higher vapor density than the spectrum shown in Figure 3. Similar to the Rb $5\,^2S_{1/2} \rightarrow 5\,^2P_{3/2}$ excitation, many atomic and molecular features are observed in the spectrum. The Rb($6\,^2P_{3/2}$) level is populated by a direct absorption of the laser light. The Rb($6\,^2P_{1/2}$) level is populated by Rb($6\,^2P_{3/2}$) and Rb($5\,^2S_{1/2}$) colissions via collisional energy transfer. In addition to the Rb($6p$) emission, lines coming from Rb($4d$), Rb($5d$), Rb($7s$) and Rb($5p$) levels are also observed. $4d$ and $5p$ atomic levels are populated by direct and cascade radiative decays of $6p$ levels, respectively. Two-photon ionization followed by radiative and three-body recombination might be an effective way to populate $7s$ and $5d$ atomic levels.

Beside diffuse band, triplet satellites, $1(B)\,^1\Pi_u \rightarrow 1(X)\,^1\Sigma_g^+$ band and $1(A)\,^1\Sigma_u^+ \rightarrow 1(X)\,^1\Sigma_g^+$ band emissions, a $3(D)\,^1\Pi_u \rightarrow 1(X)\,^1\Sigma_g^+$ band with a peak at approximately 475 nm was observed. This peak is a result of the extremum in the $3(D)\,^1\Pi_u - 1(X)\,^1\Sigma_g^+$ difference potential curve [36]. The Rb₂ $3(D)\,^1\Pi_u$ state correlates to the $5s + 6p$ molecular asymptote (see Fig. 2) and it is populated through:

(a) energy transfer from Rb($6p$) atoms to the Rb₂ molecules in the ground state

$$\mathrm{Rb}(6p) + \mathrm{Rb}_2(1(X)\,^1\Sigma_g^+) \rightarrow \mathrm{Rb}_2(3(D)\,^1\Pi_u) + \mathrm{Rb}(5s) \quad (9)$$
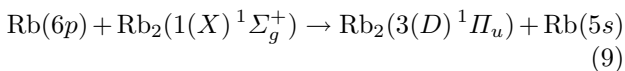
and

(b) three-body collisional recombination

$$\mathrm{Rb}(6p) + \mathrm{Rb}(5s) + \mathrm{Ar} \rightarrow \mathrm{Rb}_2(3(D)\,^1\Pi_u) + \mathrm{Ar}. \quad (10)$$

Because of the dense vapor, the first resonance D$_1$ and D$_2$ atomic lines and the molecular $B \rightarrow X$ band are self-absorbed. From Figure 3 it can be seen that a maximum of the Rb₂ $B \rightarrow X$ emission band is observed at about 690 nm. Since the absorption coefficient of the Rb₂ $X \rightarrow B$ band has a maximum at about 680 nm, in Figure 7 the Rb₂ $B \rightarrow X$ band appears self-absorbed with remaining "two bands" peaking approximately at 650 nm and 725 nm.

The detailed Rb₂ diffuse band spectrum obtained by violet laser excitation ($T = 557$ K and $p(\mathrm{Ar}) = 22$ Torr) is presented in Figure 6b (trace denoted by letter V). The diffuse band emission profile is characterized by three peaks positioned approximately at 601 nm, 603 nm and 605.5 nm. Toward the blue part of the spectrum there is also a pronounced, continuous extended wing. The diffuse band emission was observed in the temperature range from 520 K ($N_{\mathrm{Rb}} = 4.2 \times 10^{15}$ cm^{-3}) to 700 K ($N_{\mathrm{Rb}} = 2.9 \times 10^{17}$ cm^{-3}) and in the range of argon buffer gas pressures from 20 Torr to 100 Torr. The maximum emission was observed at approximately 620 K ($N_{\mathrm{Rb}} \sim 6 \times 10^{16}$ cm^{-3}) and 50 Torr of argon gas. By varying the temperature of the vapor and the argon gas pressure, the shape of the diffuse band remains unchanged. The dependence of the diffuse band intensity (peak at 601 nm) upon the power of the violet excitation laser with wavelength positioned in the near wing of the Rb D$_2$ second resonance line ($\lambda_{laser} = 420.08$ nm) shows linear behaviour (squares in Fig. 5).

We measured the excitation spectra by monitoring diffuse band emission while tuning the violet laser wavelength across the absorption profile of the Rb $5\,^2S_{1/2} \rightarrow 6\,^2P_{3/2}$ line. The violet laser wavelength tuning range of approximately 10 GHz was sufficient to scan the whole absorption profile of the Rb $5\,^2S_{1/2} \rightarrow 6\,^2P_{3/2}$ line. The dependence of the diffuse band emission peak at 601 nm, at 630 K and 72 Torr of argon gas, upon the wavelength of the excitation laser is presented in Figure 8a. Unfortunately, we were not able to calibrate the excitation $5\,^2S_{1/2} \rightarrow 6\,^2P_{3/2}$ laser wavelength scale. Therefore, in Figure 8b, we present for comparison, the excitation spectrum of the Rb $5\,^2S_{1/2} \rightarrow 6\,^2P_{1/2}$ emission line detected simultaneously. Both profiles in Figures 8a and 8b show the same self-absorbed shape of the Rb $5\,^2S_{1/2} \rightarrow 6\,^2P_{3/2}$ resonance line. Due to the low LIF signal the additional structure is produced by the noise. From Figure 8 it is obvious that the diffuse band intensity has approximately a linear dependence on the concentration of the excited Rb($6p$) atoms.

4 Discussion

As can be seen from Figure 6b, Rb₂ diffuse band emission profiles measured at the same rubidium and argon pressures show differences when excited by red (R trace)
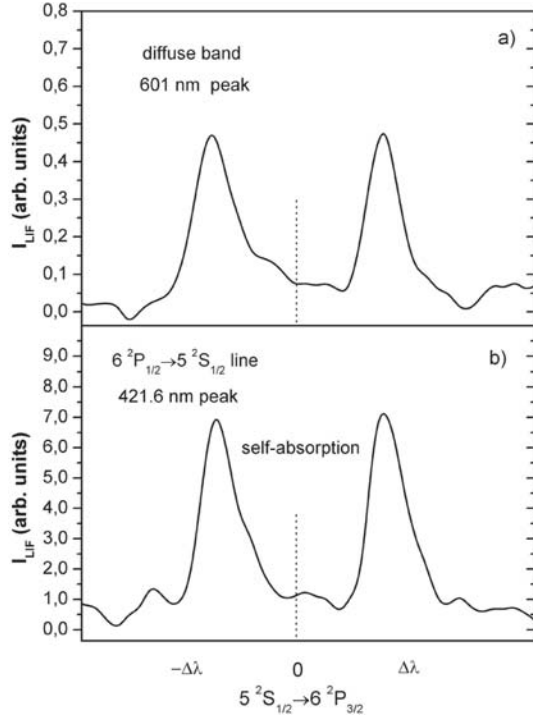
Fig. 8. Excitation spectra of (a) diffuse band – peak at 601 nm and (b) Rb $6\,^2\mathrm{P}_{1/2} \to 5\,^2\mathrm{S}_{1/2}$ second doublet resonance D_1 line – peak at 421.6 nm, obtained by tuning the violet laser wavelength across the absorption profile of the Rb $5\,^2\mathrm{S}_{1/2} \to 6\,^2\mathrm{P}_{3/2}$ second doublet resonance D_2 line. $T = 630$ K, $p(\mathrm{Ar}) = 72$ Torr.

and violet (V trace) laser radiation. The absorption coefficient obtained from the simple white light absorption measurements for rubidium vapor at 695 K is also presented in Figure 6b (trace denoted with letter A). By introducing spin-orbit interaction the Rb$_2$ $2\,^3\Pi_g$ state splits into 2_g, 1_g and degenerate $0_g^\pm$ molecular states. In Figure 6a we present the relevant difference potential curves, Rb$_2$ $2\,^3\Pi_g(2_g, 1_g, 0_g^\pm)-1(a)\,^3\Sigma_u^+ (1_u, 0_u^-)$. Each difference potential is denoted with the upper state notation. In the region of about 10 Bohr the three difference potentials exhibit minima, which are responsible for the formation of the three peaks in the diffuse band absorption spectrum (trace A in Fig. 6b). 2_g, 1_g, $0_g^\pm$ Hund's case (c) difference potentials are created from the Hund's case (a) $2\,^3\Pi_g$ potential curve [30], by adding the spin-orbit contribution $\Delta(R)(\Omega - 1)$. $\Omega = 0, 1, 2$ and $\Delta(R)$ is a semi-empirical function, which at small internuclear distances well describes the splitting of the absorption peaks. At very large distances $\Delta(R)$ corresponds to the spin-orbit splitting of the $4d + 5s$ asymptote, which is equal to 0.44 cm^{-1} [34].

The diffuse band emission profile obtained by violet laser excitation (Fig. 6b, trace V) exhibits three peaks as observed in the absorption spectrum. However, the relative intensities of these peaks are not the same as in the absorption spectrum. The diffuse band emission profile obtained by red laser excitation possesses only two peaks. This might be a consequence of the strong overlap of the second and the third peak because of their

equal intensities. An extended blue wing decreasing towards the blue part of the spectrum is obtained for the case of violet laser excitation and in the absorption spectrum. Pichler et al. [5] studied rubidium interference and diffuse continua by excitation of rubidium vapor with different c.w. argon-ion laser lines. They showed that $2\,^1\Sigma_u^+ \to 1(X)\,^1\Sigma_g^+$ emission, the so-called interference continuum, has an important influence on the shape of the diffuse band emission profile, especially in the blue part of the spectrum. On the other hand, Luh et al. [7] excited the $2\,^3\Pi_g$ state directly using a dye laser. For definite excitation wavelengths they obtained Rb$_2$ diffuse band emission spectra very similar to those obtained in this work with violet laser excitation. Our LIF measurements show that in both excitations (red and violet light) the $2\,^3\Pi_g(2_g)-1(a)\,^3\Sigma_u^+(1_u)$ transitions are the dominant ones.

From the results presented in Figures 5 and 8 we can conclude that in our experimental conditions, for both first and second D_2 resonance line excitations, the population of the Rb$_2$ $2\,^3\Pi_g$ state is related to the population of the Rb$(6p)$ excited atomic levels.

In order to describe this dependence in more detail we have measured $2\,^3\Pi_g \to 1(a)\,^3\Sigma_u^+$, I_{diff}, and $6\,^2\mathrm{P}_{3/2} \to 5\,^2\mathrm{S}_{1/2}$, I_{6p}, LIF intensities for different rubidium vapor temperatures (densities) and argon buffer gas pressures. I_{diff} and I_{6p} are measured at constant temperature of the rubidium vapor at 601 nm and 420.2 nm and they are assumed to be proportional to the concentrations of the Rb$_2(2\,^3\Pi_g)$ molecules and the Rb$(6\,^2\mathrm{P}_{3/2})$ atoms, respectively. The measurements were performed for the red light excitation laser only. In the case of the violet light excitation the scattered laser light precluded reliable measurements of I_{6p} intensity. The red excitation laser wavelength was constant during the measurements, positioned in the red wing of the Rb D_2 first resonance line (approximately at 782 nm). The non-zero values of I_{diff} and I_{6p} intensities were measured in the 495–610 K temperature range. The measured intensity ratio I_{diff}/I_{6p} as a function of the concentration of ground state rubidium atoms, for four different argon gas pressures is shown in Figure 9. The rubidium atom concentrations, N_{Rb}, were calculated from the Rb vapor pressure curve [37].

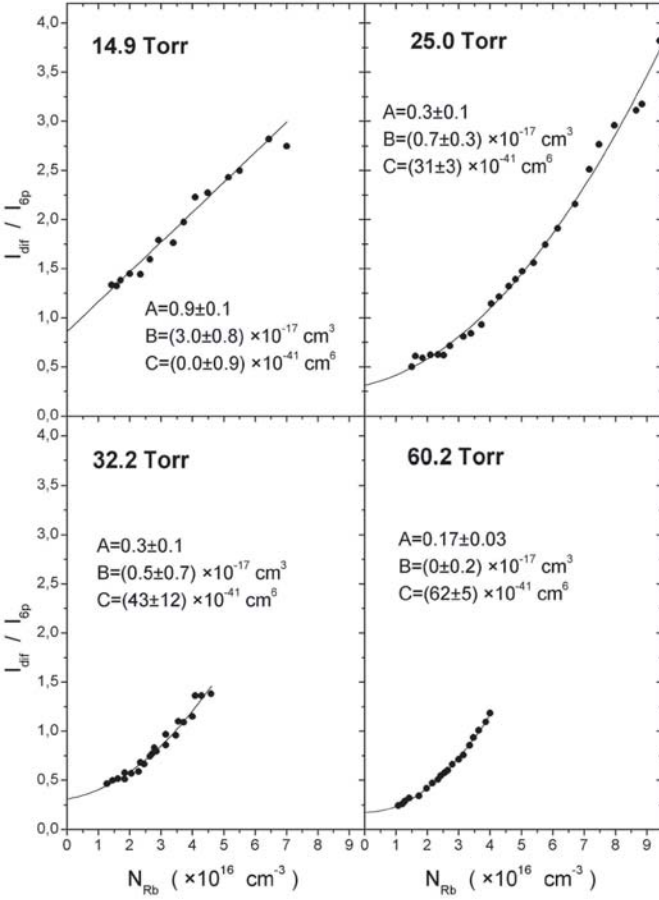The measured I_{diff}/I_{6p} intensity ratio was fitted by a second-order polynomial:

$$I_{diff}/I_{6p} = A + BN_{\mathrm{Rb}} + CN_{\mathrm{Rb}}^2, \qquad (11)$$

at each argon gas pressure. A, B and C coefficients depend on the argon gas pressure (Fig. 10).

Each term in equation (11) corresponds to a different Rb$_2(2\,^3\Pi_g)$ state population mechanism. We assume that the BN_{Rb} term reflects the population of the Rb$_2(2\,^3\Pi_g)$ molecular state through its Rb$(5s)$ + Rb$(4d)$ asymptote (atomic channel):

$$\mathrm{Rb}(5s) + \mathrm{Rb}(4d) + M \to \mathrm{Rb}_2(2\,^3\Pi_g) + M, \qquad (12)$$

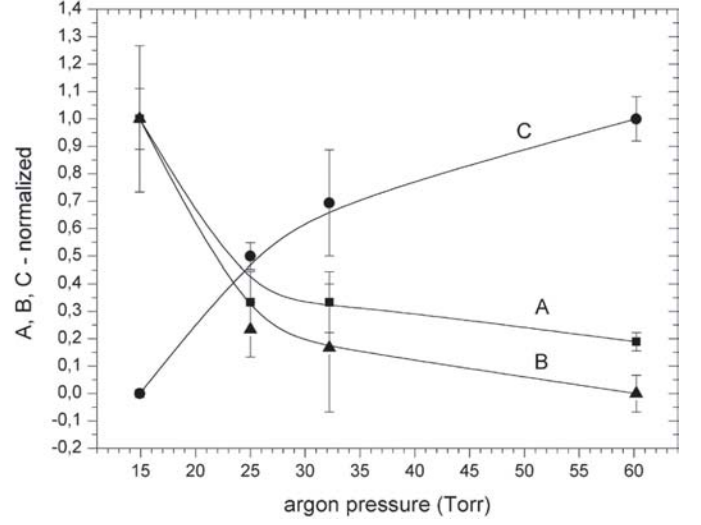where M denotes the argon gas atom, Ar, or the rubidium atom in the ground state, Rb$(5s)$. The concentration
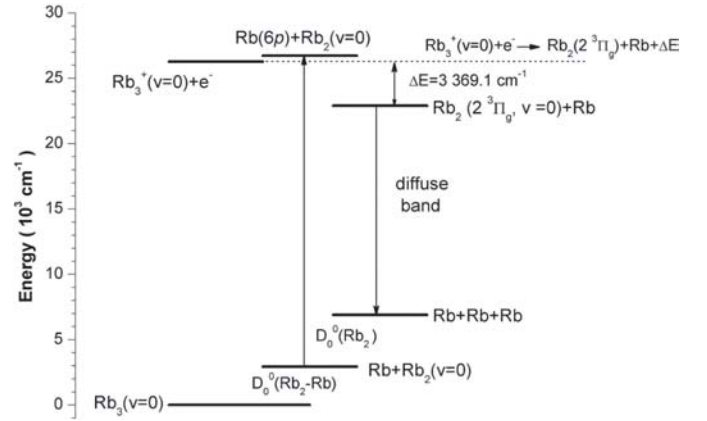
Fig. 9. The measured intensity ratio I_{diff}/I_{6p} as a function of the concentration of ground state rubidium atoms, N_{Rb}, for four different argon gas pressures.
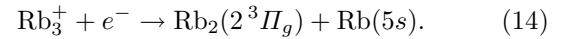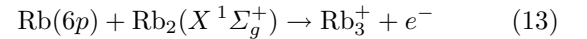

Fig. 10. Normalized values of A, B and C coefficients as a function of the argon gas pressure. A – squares, B – triangles and C – circles.


Fig. 11. Rubidium three atom energy diagram. D_0^o (Rb$_2$–Rb) – rubidium trimer dissociation energy, D_0^o (Rb$_2$) – rubidium dimer dissociation energy.

of the Rb($4d$) atoms is proportional to the concentration of the Rb($6p$) atoms because the Rb($4d$) level is predominately populated by radiative decay from the Rb($6p$) level. The Rb$_2(2\,^3\Pi_g)$ state is populated by Rb($4d$) and Rb($5s$) inelastic collisions (in the presence of the third particle). Depopulation of the Rb$_2(2\,^3\Pi_g)$ molecular state by radiative decay, results in the observed diffuse band emission. The population of the lithium diffuse band through its asymptote is discussed in reference [38].

The alkali vapor consists of alkali atoms and a few percent of diatomic alkali molecules with the concentrations given by $N_{\text{Rb}_2} = K(T)N_{\text{Rb}}^2$. Therefore, quadratic CN_{Rb}^2 term in equation (11) suggests that the Rb$_2$ ground state molecules, N_{Rb_2}, also participate in the Rb$_2(2\,^3\Pi_g)$ state population. One of the most probable mechanism in which Rb($6p$) atoms and Rb$_2$ ground state molecules could populate the Rb$_2(2\,^3\Pi_g)$ excited state is connected with the creation of the Rb$_3^+$ ions in the vapor. Associative ionization to the trimer ion (relation (7)) is energetically possible (see Fig. 4). The lowest atomic limit above the threshold for two-body associative ionization to the trimer ion is Rb($6\,^2\text{P}_{1/2}$) atomic level. The Rb$_3^+$ molecular ion undergoes dissociative recombination to the Rb$_2(2\,^3\Pi_g)$ ex-

cited molecule and Rb($5s$) atom, with an excess energy of 3369.1 cm^{-1}

$$\text{Rb}(6p) + \text{Rb}_2(X\,^1\Sigma_g^+) \rightarrow \text{Rb}_3^+ + e^- \qquad (13)$$

$$\text{Rb}_3^+ + e^- \rightarrow \text{Rb}_2(2\,^3\Pi_g) + \text{Rb}(5s). \qquad (14)$$

Relations (14) and (15) can be symbolically summarized by the following collision energy transfer process (molecular channel):

$$\text{Rb}(6p) + \text{Rb}_2(X\,^1\Sigma_g^+) \rightarrow \text{Rb}_2(2\,^3\Pi_g) + \text{Rb}(5s). \qquad (15)$$
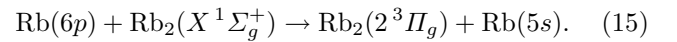
In Figure 11 we describe the three atom energy cycle. This three atom energy cycle together with the energy data needed for its creation were taken from reference [22]. By changing argon gas pressure from 14.9 Torr to 60.2 Torr, the coefficients A (offset) and B (linear term in N_{Rb}) decrease toward zero. Simultaneously, the coefficient C (quadratic term in N_{Rb}) increases from zero. Normalized

values of A, B and C coefficients as a function of the argon gas pressure are shown in Figure 10. The relative increase of the C with the Ar pressure and the decrease of the B suggest that a presence of the buffer gas atoms favors the molecular channel for the formation of the $2\,^3\Pi_g$ state. Although one would expect that higher buffer gas pressure would enhance the atomic channel because of the enhanced rate of the three-body collisions, we observed the decrease in atomic channel contribution and increase in molecular channel contribution with increasing pressure. This discrepancy calls for a more elaborate model for the population of the $2\,^3\Pi_g$ state, but we firmly believe that both mechanisms for population of the $2\,^3\Pi_g$ state are present for the given experimental condition.

Unfortunately, the physical meaning of the offset A in equation (11) remains unclear. Several different sources can affect the offset A: (a) systematic error in determination of the temperature of the rubidium vapor, (b) the population of $Rb_2(2\,^3\Pi_g)$ state through different collision channels independent of the $Rb(6p)$ atoms concentration, (c) $6\,^2P_{1/2} \rightarrow 6\,^2P_{3/2}$ fine-structure changing collisions and (d) radiation trapping.

5 Conclusion

We observed the Rb_2 orange color diffuse band by laser excitation of the rubidium first and second resonance doublet. It is obvious that the $Rb_2(2\,^3\Pi_g)$ state can not be populated directly by absorption of the applied red or violet laser light. Therefore, significant Rb_2 diffuse band emission intensity points to the conclusion of effective collisional energy transfer processes involved in the $Rb_2(2\,^3\Pi_g)$ state population. We indicated that in both cases of excitation (red and violet laser) the population of the $Rb_2(2\,^3\Pi_g)$ state is correlated to the concentration of the $Rb(6p)$ atoms in the vapor.

From I_{diff}/I_{6p} versus N_{Rb} measurements we speculated about two different $Rb_2(2\,^3\Pi_g)$ state population mechanisms. We connected the first one, linear in N_{Rb}, with the population of $Rb_2(2\,^3\Pi_g)$ molecular state through its corresponding molecular asymptote, $Rb(5s)+Rb(4d)$. The second one, quadratic in N_{Rb}, is a result of atom-molecule energy transfer, probably mediated by the Rb_3^+ ions. In our experimental conditions, the efficiency of the proposed mechanisms depends on the rubidium vapor density and argon buffer gas density.

Further steps in our investigation will be concentrated on the direct experimental detection of the Rb_3^+ molecular ions. This is a highly interesting and complex problem, which requires special experimental efforts. In addition, the knowledge of theoretical potential energy surfaces for this particular molecular ion will certainly be of much help in all subsequent analyses.

References

1. R. Gupta et al., J. Chem. Phys. **68**, 799 (1978)
2. G. Pichler et al., J. Phys. B: At. Mol. Phys. **16**, 4619 (1983)
3. J.M. Brom Jr, H.P. Broida, J. Chem. Phys. **61**, 962 (1974)
4. S. Milošević, in *The Physics of Ionized Gases, Spig 88*, 1988, edited by L. Tanović, N. Konjević, N. Tanović (Nova Science Publishers, New York, 1988), p. 517
5. G. Pichler et al., J. Phys. B: At. Mol. Phys. **16**, 4633 (1983)
6. J.T. Bahns, W.L. Stwalley, G. Pichler, J. Chem. Phys. **90**, 2841 (1989)
7. W.-T. Luh et al., J. Chem. Phys. **88**, 2235 (1998)
8. J.P. Woerdman, Opt. Commun. **26**, 216 (1978)
9. D. Xing, K. Ueda, H. Takuma, Appl. Phys. Lett. **60**, 2960 (1992)
10. J.T. Bahns, W.C. Stwalley, Appl. Phys. Lett. **44**, 826 (1984)
11. H.H. Wu, T.C. Chu, C.Y.R. Wu, Appl. Phys. B **43**, 225 (1987)
12. A. Fioretti et al., Phys. Rev. Lett. **80**, 4402 (1998)
13. A. Fioretti et al., Eur. Phys. J. D **15**, 189 (2001)
14. C.M. Dion et al., Eur. Phys. J. D **18**, 365 (2002)
15. G. Pichler, in *CP645, Spectral Line Shapes*, 2002, edited by C.A. Back (American Institute of Physics, New York, 2002), Vol. 12, p. 487
16. S. Milošević et al., Chem. Phys. Lett. **128**, 145 (1986)
17. S. Milošević, G. Pichler, Z. Phys. D **1**, 223 (1986)
18. L.T. Xiao et al., Appl. Phys. B **68**, 727 (1999)
19. Zh.L. Shvegzhda, S.M. Papernov, M.L. Janson, Chem. Phys. Lett. **101**, 187 (1983)
20. D. Veža, S. Milošević, G. Pichler, Opt. Commun. **56**, 172 (1985)
21. Yu.P. Korchevoi, V.I. Lukashenko, S.N. Lukashenko, Phys. Scripta **19**, 271 (1979)
22. W.C. Stwalley, J.T. Bahns, Laser Part. Beams **11**, 185 (1993)
23. C. Tapalian, W.W. Smith, Chem. Phys. Lett. **211**, 425 (1993)
24. G. Pichler et al., Chem. Phys. Lett. **129**, 425 (1986)
25. A. Ekers et al., Chem. Phys. Lett. **304**, 69 (1999)
26. J. Klavins et al., Chem. Phys. Lett. **228**, 346 (1994)
27. J. Huennekens, Z. Wu, T.G. Walker, Phys. Rev. A **31**, 196 (1985)
28. A. Hemmerich et al., Opt. Commun. **75**, 118 (1990)
29. R.S. Conroy et al., Opt. Commun. **175**, 185 (2000)
30. F. Spiegelmann, D. Pavolini, J.-P. Daudey, J. Phys. B: At. Mol. Opt. Phys. **22**, 2465 (1989)
31. L. Barbier, M. Chéret, J. Phys. B: At. Mol. Phys. **16**, 3213 (1983)
32. A. Ekers et al., Can. J. Phys. **79**, 1039 (2001)
33. Č. Vadla (private communication)
34. C.E. Moore, *Atomic Energy Levels*, NSRDS-NBS **35**, 125 (1971)
35. M.-L. Almazor et al., Eur. Phys. J. D **15**, 355 (2001)
36. E.J. Breford, F. Engelke, Chem. Phys. Lett. **75**, 132 (1980)
37. A.N. Nesmeyanov, *Vapor Pressures of Chemical Elements* (Elsevier, New York, 1963)
38. D. Veža, C.J. Sansonetti, Z. Phys. D **22**, 463 (1992)